Association of condensin with chromosomes depends on DNA binding by its HEAT-repeat subunits

Ilaria Piazza[1,2,3], Anna Rutkowska[1,2], Alessandro Ori[2], Marta Walczak[1,2,5], Vicent Pelechano[4], Martin Beck[2] & Christian H. Haering[1,2,6]

[1] Cell Biology & Biophysics Unit, European Molecular Biology Laboratory (EMBL), Heidelberg, Germany

[2] Structural & Computational Biology Unit, European Molecular Biology Laboratory (EMBL), Heidelberg, Germany

[3] International PhD Programme, European Molecular Biology Laboratory (EMBL), Heidelberg, Germany

[4] Genome Biology Unit, European Molecular Biology Laboratory (EMBL), Heidelberg, Germany

[5] Present address: Max F. Perutz Laboratories, Vienna, Austria

[6] Correspondence: christian.haering@embl.de

Condensin complexes play central roles in the three-dimensional organization of chromosomes during cell divisions, but how they interact with chromatin to promote chromosome segregation is largely unknown. Previous work suggested that condensin, in addition to encircling chromatin fibers topologically within the ring-shaped structure formed by its SMC and kleisin subunits, contacts DNA directly. Here we describe the discovery of a binding domain for double-stranded DNA formed by the two HEAT-repeat subunits of the *Saccharomyces cerevisiae* condensin complex. Based on detailed mapping data of the interfaces between the HEAT-repeat and kleisin subunits, we generated condensin complexes that lack one of the HEAT-repeat subunits and consequently fail to associate with chromosomes in yeast and human cells. The finding that DNA binding by condensin's HEAT-repeat subunits stimulates the SMC ATPase activity suggests a multi-step mechanism for the loading of condensin onto chromosomes.

Introduction

The segregation of eukaryotic and prokaryotic chromosomes during cell divisions depends on the action of multi-subunit protein complexes named condensins. Despite their early emergence during evolution as universal chromosome organizers, it has remained largely unknown how condensins structure mitotic and meiotic chromosomes into rigid rod-shaped shapes[1,2] or help to disentangle and partition replicated sister DNAs[3]. Similarly little is known about molecular mechanisms behind the increasing number of roles eukaryotic condensin complexes play in chromatin organization during interphase, gene regulation, and DNA damage repair[4]. A major reason for the lack of understanding condensin function is that the interaction of the complex with its chromosome substrates has not yet been well defined.

Condensin complexes are composed of five core subunits[5]. Condensin's Smc2 (CAP-E) and Smc4 (CAP-C) subunits belong to the structural maintenance of chromosomes (SMC) protein family, whose members are characterized by a central ~45 nm long anti-parallel coiled coil that separates a 'hinge' dimerization domain at one end from the ATPase 'head' domain formed by the protein's N and C termini at the other end. Smc2 and Smc4 associate via their hinge domains and in addition, upon sandwiching two molecules of ATP in-between them, via their ATPase

head domains [6]. A subunit of the kleisin protein family[7] connects the Smc2 and Smc4 ATPase head domains, presumably by simultaneously binding to the Smc2 head via its N-terminal helix-turn-helix (HTH) motif and to the Smc4 head via its C-terminal winged helix domain (WHD)[8]. In addition to binding Smc2 and Smc4, the kleisin subunit recruits to the complex two proteins that are predicted to be largely composed of α-helical HEAT (Huntingtin, Elongation factor 3, protein phosphatase 2A, Tor1 kinase) repeat motives (Fig. 1a)[8,9]. In the budding yeast *Saccharomyces cerevisiae*, the kleisin subunit Brn1 forms a single non-SMC subcomplex with the HEAT-repeat subunits Ycs4 and Ycg1. In human cells, the Smc2–Smc4 dimer associates with two distinct non-SMC subcomplexes. Condensin I contains the γ-kleisin CAP-H and the HEAT-repeat subunits CAP-D2 and CAP-G, condensin II contains the β-kleisin CAP-H2 and the HEAT-repeat subunits CAP-D3 and CAP-G2[10].

Condensin holocomplexes isolated from meiotic *Xenopus laevis* egg extracts are able to bind to and, remarkably, change the topological and supercoiling states of circular plasmid DNAs in the presence of topoisomerases *in vitro*[11,12]. Individual *Xenopus* Smc2–Smc4 or non-SMC subcomplexes, in contrast, bind to DNA only at very low salt conditions, fail to associate with chromatin in cell extracts, and cannot promote changes in DNA topology or support the transformation into rod-shaped chromosomes of chromatin added to meiotic frog egg extracts[13]. Budding and fission yeast Smc2–Smc4 dimers, on the contrary, have been reported to bind to DNA and, in the case of the former, induce the formation of knotted structures into plasmid DNA in an analogous

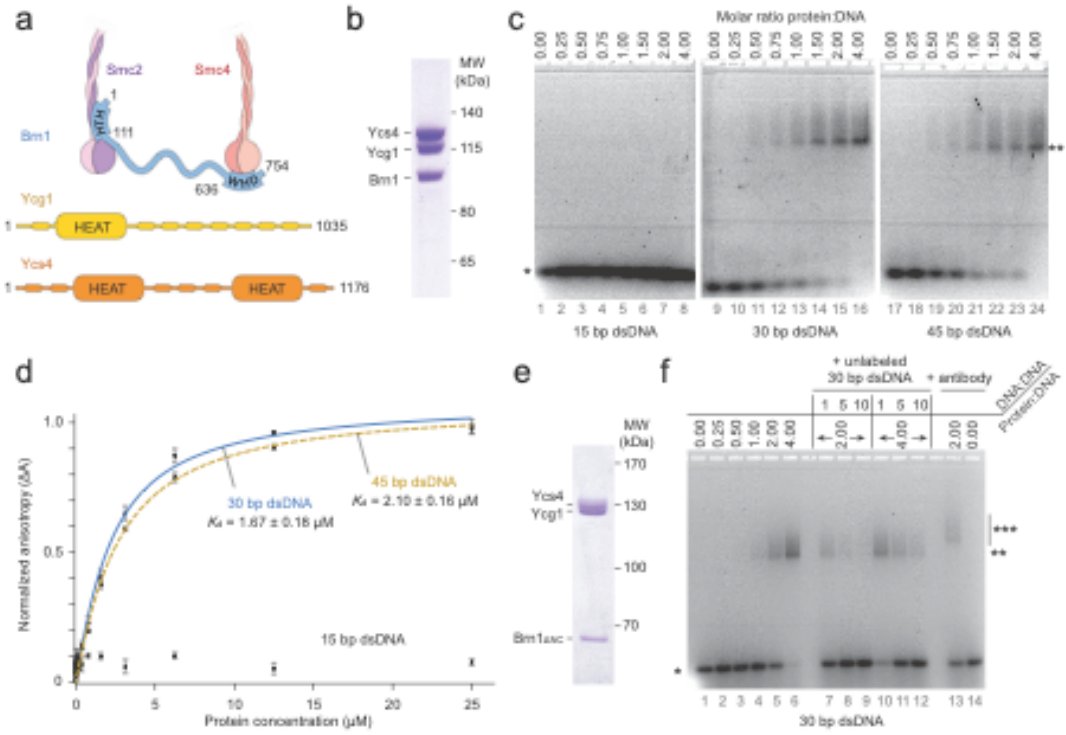

Figure 1 DNA binding by condensin non-SMC subcomplexes. (**a**) Schematic representation of the five condensin subunits labeled with the *S. cerevisiae* protein names. Amino acid residue numbers and positions of the helix-turn-helix (HTH) motif, winged helix domain (WHD), and blocks of HEAT repeats are indicated. Small ovals indicate regions rich in α-helices. (**b**) Analysis of Brn1–Ycs4–Ycg1 after gelfiltration by SDS PAGE and Coomassie staining. (**c**) Electrophoretic mobility shift assay of 15–45 bp dsDNA substrates, using 0.2 μM 6-FAM-labeled dsDNA in the presence of 0.0–0.8 μM Brn1–Ycs4–Ycg1. Unbound (*) and slower migrating species (**) are indicated. (**d**) Binding affinities of Brn1–Ycs4–Ycg1 to 15–45 bp 6-FAM-labeled dsDNA substrates were determined by measuring fluorescence anisotropy changes ΔA upon addition of the indicated protein concentrations. Dissociation constants (K_d) were calculated by fitting mean ΔA values for each protein concentration assuming a single-site binding model. Points and error bars indicate mean and s. d. of $n = 3$ technical replicates. (**e**) Analysis of purified $Brn1_{\Delta C}$–Ycs4–Ycg1 as in **b**. Note that the central region of Brn1 stains only weakly with Coomassie. (**f**) Electrophoretic mobility shift assay of a 30 bp dsDNA with $Brn1_{\Delta NC}$–Ycs4–Ycg1 as in **c** (lanes 1–6) after addition of unlabeled 30 bp competitor DNA (lanes 7–12) or an antibody against the His_6 tag on Ycs4 (lanes 13–14). Unbound (*), slower migrating (**), and antibody super-shifted (***) species are indicated. Panels **c** and **f** show one representative experiment of $n = 3$ independent replicates.

manner to the *Xenopus* condensin holocomplex[14-16]. These findings are consistent with the suggestion that condensin's major DNA binding activity might be exerted by the Smc2–Smc4 subcomplex, which is either enhanced[13] or diminished[16] by the non-SMC subcomplex. Since an isolated Smc2–Smc4 hinge domain, like the Smc1–Smc3 hinge domain of the condensin-related cohesin complex[17] and the hinge domains of prokaryotic SMC homodimers [18-20], is able to induce an electrophoretic mobility shift of various DNA constructs[21], it might form the primary contact point for DNA binding. Atomic force microscopy (AFM) images of condensin–DNA complexes furthermore support this conclusion[22]. However, the strong preference for binding single-stranded DNA (ssDNA) over double-stranded DNA (dsDNA) substrates implies that the DNA binding activity of the hinge domain might fulfill specialized roles, such as promoting ssDNA annealing during DNA damage repair or transcription[21,23,24].

An alternative hypothesis for how condensin complexes bind to DNA comes from the finding that DNA linearization or proteolytic opening of the tripartite ring structure formed by the Smc2, Smc4, and kleisin subunits releases the association between yeast condensin and circular minichromosomes *in vitro* and, in the case of the latter, between condensin and chromosomes *in vivo*[25]. Condensin rings might therefore encircle chromatin fibers topologically in a similar manner as cohesin rings entrap sister chromatids[26]. Interestingly, efficient release of condensin from minichromosomes required substantially higher salt concentrations than release of cohesin[25], suggesting that condensin might make additional direct protein-chromatin contacts with DNA (see above) or with histones[27,28].

While all existing models propose defined tasks in DNA binding for the condensin SMC and kleisin components, the role of the two HEAT-repeat subunits has remained enigmatic. To gain insights into their contribution to condensin function, we biochemically characterized the two proteins as part of the condensin non-SMC subcomplex and discovered that the non-SMC subcomplex forms a specific binding domain for dsDNA substrates. Mapping of the binding of both HEAT-repeat subunits to the kleisin protein by cross-linking mass spectrometry and co-purification experiments allowed us to specifically prevent assembly of Ycg1, CAP-G, or CAP-G2 subunits into yeast and human condensin complexes, respectively. Such tetrameric complexes failed to associate with mitotic chromosomes. Finally, we found that binding of DNA to the non-SMC subcomplex strongly stimulates the ATPase activity of the Smc2–Smc4 dimer. Our findings suggest that DNA binding by the non-SMC subcomplex and activation of the SMC ATPase activity constitute the first two steps in the topological loading of condensin rings onto chromosomes.

Results

The condensin non-SMC subcomplex binds DNA

To investigate the properties of the condensin non-SMC subcomplex, we co-expressed in insect cells and purified to homogeneity the kleisin subunit Brn1 and the HEAT-repeat subunits Ycg1 and Ycs4 from *Saccharomyces cerevisiae* (Supplementary Fig. 1a and Supplementary Table 1). The vast majority of Brn1, Ycg1, and Ycs4 co-eluted during gelfiltration chromatography (Supplementary Fig. 1b). Coomassie staining of the peak elution fraction indicated that all three subunits were present at equimolar stoichiometry (Fig. 1b). Electron micrographs of the negatively stained Brn1–Ycs4–Ycg1 subcomplexes showed isolated particles with a spherical shape of ~20 nm diameter (Supplementary Fig. 1c), consistent with the predicted size for a 1:1:1 complex of 340 kDa molecular weight.

Since previous evidence suggested that condensin makes direct contacts with chromatin, we tested whether the non-SMC subcomplex might provide a platform for DNA binding. Indeed, addition of the Brn1–Ycs4–Ycg1 subcomplex to a linearized plasmid altered the migration of the plasmid DNA during gel electrophoresis (Supplementary Fig. 2a). To characterize this interaction with defined DNA substrates, we incubated Brn1–Ycs4–Ycg1 with dsDNA oligonucleotide substrates of 15-45 bp lengths, which we had labeled with 6-carboxyfluorescein

(6-FAM) to allow their detection in a gelshift experiment (Supplementary Fig. 2b). While addition of the non-SMC complex did not notably affect the electrophoretic mobility of the 15 bp dsDNA (Fig. 1c, lanes 1-8), it resulted in the formation of a slower-migrating species with 30 or 45 bp dsDNA substrates already at substoichiometric protein:DNA ratios (Fig. 1c, lanes 9-24). The mobility shift of the 30 bp dsDNA (Supplementary Fig. 2c, lanes 1-6) could be reverted by addition of a 10-fold excess of unlabeled dsDNA (Supplementary Fig. 2c, lanes 7-12) and was augmented by the addition of an antibody against the His_6 epitope fused to Ycs4 (Supplementary Fig. 2c, lanes 13 and 14). These data are consistent with a specific and reversible binding of the non-SMC subcomplex to short DNA substrates. We then used a fluorescence anisotropy assay to estimate the binding affinities between the Brn1–Ycs4–Ycg1 subcomplex and DNA in solution (Fig. 1d). We measured low-micromolar affinities for binding of the non-SMC subcomplex to the 30 and 45 bp dsDNA substrates ($K_d \approx 2$ µM). Finally, we confirmed that binding to the 30 bp dsDNA also altered the migration of the non-SMC subcomplex during native protein gel electrophoresis (Supplementary Fig. 2d).

The finding that the condensin non-SMC subcomplex efficiently binds to DNA was surprising, since the only predicted *bona fide* DNA binding motives present in the subcomplex are the HTH and WHD motives at the N and C termini of the kleisin subunit [29]. In kleisin proteins, both motives are, however, involved in binding to the SMC head domains[30-32]. To test whether these motives were responsible for the observed DNA gelshift, we co-expressed a truncated version of Brn1 that lacks both motives ($Brn1_{\Delta NC}$) with Ycg1 and Ycs4. These three proteins also formed a stable complex (Fig. 1e), which eluted from the final gelfiltration step at a slightly higher elution volume than the trimeric complex containing full-length Brn1,

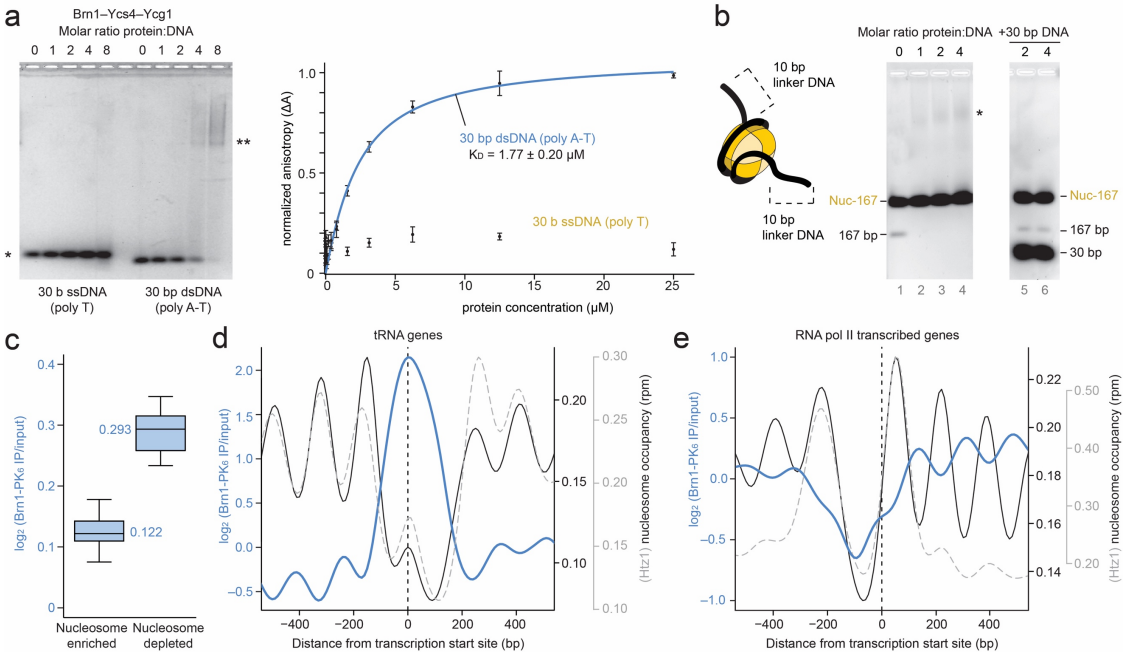

Figure 2 DNA and chromosome binding properties of the non-SMC subcomplex. (**a**) Electrophoretic mobility shift and fluorescence anisotropy binding assays of 6-FAM-labeled 30 bp dsDNA and ssDNA substrates with increasing Brn1–Ycs4–Ycg1 concentrations. Unbound (*) and slower migrating species (**) are indicated. Points and error bars indicate mean and s. d. of $n = 3$ independent experiments. (**b**) Electrophoretic mobility shift assay of a 167 bp DNA assembled into a nucleosome (Nuc-167) and a small fraction (~2%) of free 167 bp DNA with increasing Brn1–Ycs4–Ycg1 concentrations before and after addition of a 10-fold excess of 30 bp competitor dsDNA. Upshifted free 167 bp DNA (*) is indicated. (**c**) Brn1-PK_6 ChIP-seq reads from yeast strain C3632 were assigned to nucleosome-enriched or -depleted regions of the budding yeast genome; $P < 4\times10^{-9}$, Wilconox two-sided test. (**d**) Metagene analysis for the transcription start site (vertical dashed line) of all *S. cerevisiae* protein coding genes. Condensin (blue line) expressed as enrichment over the input and average nucleosome (black line) or histone H2A.Z nucleosome (dashed grey line) occupancy expressed in reads per million (rpm) were computed for each 10 bp bin and are represented by smoothing splines. (e) Metagene analysis for all *S. cerevisiae* tRNA genes as in **d**. Panels **a** and **b** show one representative experiment of $n = 3$ independent replicates.

consistent with its reduced molecular mass of 303 kDa (Supplementary Fig. 1c and 1d). The Brn1$_{\Delta NC}$–Ycs4–Ycg1 subcomplex bound plasmid DNA (Supplementary Fig. 2e) and 30 bp dsDNA (Fig. 1f) with the same or even slightly higher efficiency than the subcomplex containing full-length Brn1 (Supplementary Fig. 2f). We conclude that the non-SMC subcomplex binds to short dsDNA substrates with low micromolar affinity, most likely via its HEAT-repeat subunits.

Selected binding of double-stranded DNA helices

The Smc2–Smc4 dimer of condensin had previously been reported to bind to DNA via its hinge domain[21,22]. We therefore compared binding to single- and double-stranded DNAs of the Smc2–Smc4 hinge and the non-SMC subcomplex (Supplementary Fig. 3a). While the Brn1–Ycs4–Ycg1 complex bound to a 30 bp A-T dsDNA substrate with similar affinity ($K_d \approx 2$ μM) as to the random 30 bp dsDNA sequence used before, we could not detect binding to a 30-mer poly T ssDNA substrate (Fig. 2a). In contrast, addition of the Smc2–Smc4 hinge dimer to ssDNA and dsDNA produced, at high protein:DNA ratios (≥ 16:1), complexes that failed to enter the gel, possibly because of the highly positively charged surface of the Smc2–Smc4 hinge domain (*pI* = 9.3). In the fluorescence anisotropy assay, we measured binding of the hinge domain with low-micromolar affinity ($K_d \approx 0.3$ μM) to ssDNA but not to dsDNA (Supplementary Fig. 3b), consistent with what has been reported for the mouse Smc2–Smc4 hinge domain[21]. The fact that pre-formed complexes between the Smc2–Smc4 hinge and dsDNA were outcompeted by addition of a sub-stoichiometric amount of Brn1–Ycs4–Ycg1 (Supplementary Fig. 3c) furthermore supports the conclusion that the non-SMC subcomplex binds to dsDNA with appreciably higher affinity than the Smc2–Smc4 hinge domain. This experiment also suggests that the non-SMC subcomplex binds dsDNA with little or no DNA sequence specificity, since two very different 30 bp dsDNA ligands showed similar binding affinities (Fig. 1d and 2a).

Since the kleisin subunits of fission yeast and human condensin (I) complexes have been reported to directly interact with histone H2A and H2A.Z tails[27], we also tested binding of the non-SMC subcomplex to nucleosomes reconstituted *in vitro* from yeast histones and a 167 bp dsDNA[33] (Fig. 2b and Supplementary Fig. 3d). While we could not detect an electrophoretic mobility shift of the nucleosomal DNA, the band corresponding to a small fraction of 167 bp DNA that had not been incorporated into nucleosomes was no longer detectable upon addition of the non-SMC subcomplex, but re-appeared after addition of a 10-fold molar excess of 30 bp dsDNA (Fig. 2b). The condensin non-SMC subcomplex therefore binds with strong preference free over nucleosomal DNA. The 10 bp linker DNA overhangs at the nucleosome entry and exit sites present in the 167 bp nucleosome are obviously not sufficient for stable association with the non-SMC subcomplex. The tendency for condensin's association with free over nucleosome-bound DNA became furthermore apparent when we

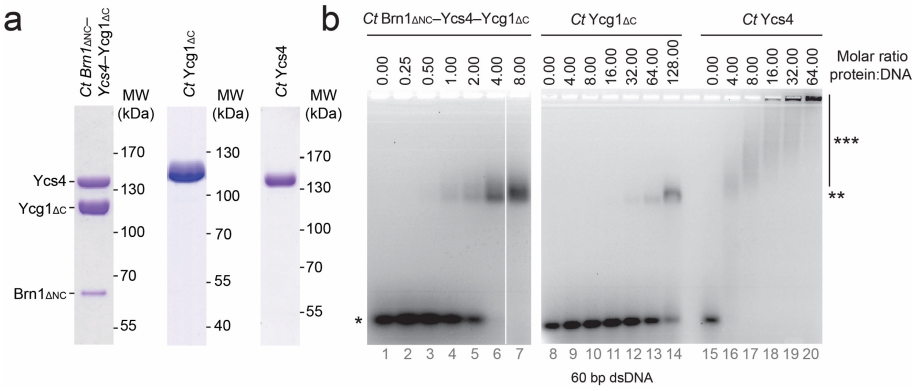

Figure 3 Both HEAT-repeat subunits are necessary for efficient dsDNA binding. (**a**) Purified *C. thermophilum* Brn1$_{\Delta NC}$–Ycs4–Ycg1$_{\Delta C}$ complex, *Ct* Ycg1$_{\Delta C}$, and *Ct* Ycs4 were analyzed by SDS PAGE and Coomassie staining. (**b**) Electrophoretic mobility shift assay of a 6-FAM-labeled 60 bp dsDNA at increasing concentrations of *Ct* Brn1$_{\Delta NC}$–Ycs4–Ycg1$_{\Delta C}$, *Ct* Ycg1$_{\Delta C}$, or *Ct* Ycs4. Unbound (*), *Ct* Brn1$_{\Delta NC}$–Ycs4–Ycg1$_{\Delta C}$ or *Ct* Ycg1$_{\Delta C}$-bound (**), and *Ct* Ycs4-bound complexes (***) are indicated. Panel **b** shows one representative experiment of $n = 3$ independent replicates.

compared by chromatin immunoprecipitation and massive parallel sequencing (ChIP-seq) the genome-wide distribution of budding yeast condensin (see below and ref. 34) with that of nucleosomes in general[35] (Fig. 2c) or histone H2A.Z-containing nucleosomes in particular[36] (Supplementary Fig. 3e and f). The preference of condensin localization to nucleosome-free regions was very obvious at the promoters of tRNA genes transcribed by RNA polymerase III (Fig. 2d), but surprisingly not of RNA polymerase II-transcribed genes (Fig. 2e). Nevertheless, at both classes of genes condensin binding patterns appeared to anti-correlate with nucleosome binding patterns. Thus, binding of the non-SMC complex to free DNA helices *in vitro* reflects the preferred positioning of condensin complexes *in vivo*.

Efficient DNA binding requires both HEAT-repeat subunits

We next tested whether either of the two condensin HEAT-repeat subunits is capable of binding DNA individually. Since we could not purify the individual *S. cerevisiae* HEAT-repeat subunits in sufficient amounts and quality, we expressed and purified to homogeneity the Ycs4 and Ycg1 subunits from the thermophilic yeast *Chaetomium thermophilum* (*Ct*)[37] and compared their DNA binding activities to that of the *Ct* non-SMC subcomplex (Fig. 3a, Supplementary Fig. 4, and Supplementary Table 1). In gelshift experiments, addition of *Ct* Brn1$_{\Delta NC}$–Ycs4–Ycg1$_{\Delta C}$ to a 60 bp dsDNA substrate produced a discrete slow-migrating band (Fig. 3b, lanes 1-7), similar to what we had observed for the *S. cerevisiae* Brn1$_{\Delta NC}$–Ycs4–Ycg1 subcomplex (Fig. 1f). *Ct* Ycg1, in contrast, shifted just a fraction of the 60 bp dsDNA substrate into a discrete band at high protein:DNA ratios (Fig. 3b, lanes 8-14). Addition of *Ct* Ycs4 to the 60 bp dsDNA produced a diffuse streak of slower

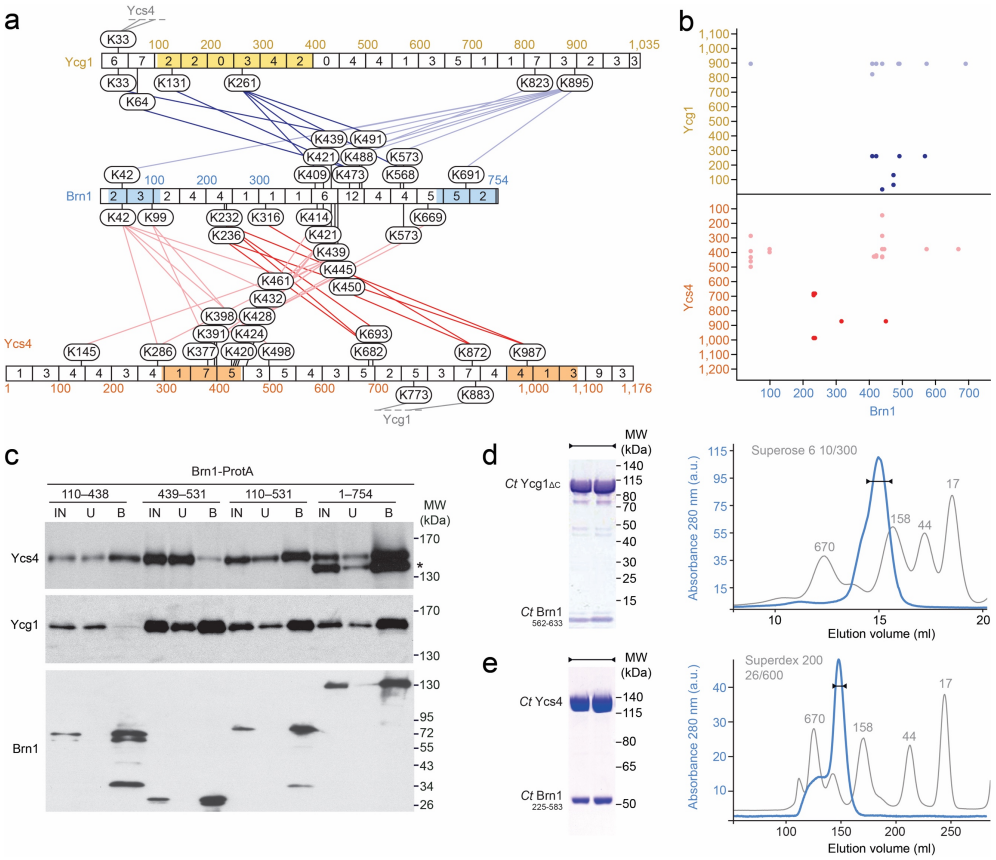

Figure 4 Subunit geometry of the non-SMC subcomplex. (**a**) Linkage map showing the positions of all high-confidence inter-subunit links identified in the *S. cerevisiae* non-SMC subcomplex by cross-linking and mass spectrometry. The numbers of lysine residues present in windows of 50 residues are indicated in squared boxes; HEAT-repeat, HTH, and WHD motives are indicated in color. Cross-links between the N or C termini of Ycg1 with Brn1 are indicated by dark or light blue lines, respectively; cross-links between the N or C termini of Ycs4 with Brn1 are indicated by pink or red lines, respectively. (**b**) Scatter plot graph of the cross-links described in **a**. Residue numbers are indicated on the axes. (**c**) Fragments of the indicated residue range of Brn1 were expressed as Protein A fusion proteins in *S. cerevisiae*. Co-purification of endogenous condensin subunits on IgG beads was probed by western blotting against the PK$_9$ tag on Ycs4 or the HA$_6$ tag on Ycg1 in input (IN), unbound (U), and 10× bound (B) fractions. A band that results from binding of the anti-PK antibody by the full-length Brn1-ProtA in indicated by an asterisk (*). (**d**) SDS-PAGE and Coomassie staining of the *Ct* Brn1$_{562-633}$–Ycg1$_{\Delta C}$ complex after Ni-NTA, ion exchange chromatography, and gelfiltration chromatography (graph). (**e**) Purification of a stable *Ct* Brn1$_{225-583}$–Ycs4 complex as in **d**.

migrating species that accumulated in the well of the gel at high protein:DNA ratios (Fig. 3b, lanes 15-20). These results suggest that the two individual condensin HEAT-repeat subunits are able to interact with DNA, albeit with considerably lower affinity than when they are combined in the non-SMC subcomplex.

Subunit geometry of the condensin non-SMC subcomplex

To gain insights into the three-dimensional organization of the *S. cerevisiae* non-SMC subcomplex, we generated an interaction map of its three subunits using a cross-linking mass spectrometry approach[38,39]. Following chemical cross-linking with disuccinimidyl suberate (DSS) at conditions that did not result in inter-complex cross-links (Supplementary Fig. 5a), we mapped cross-linked lysine residues by tandem mass-spectrometry (Supplementary Fig. 5b). This analysis identified 45 unique inter-subunit and 48 intra-subunit cross-links (Supplementary Tables 2 and 3). Remarkably, out of the 45 inter-subunit cross-links, only two connected Ycs4 with Ycg1, while 27 or 16 links connected Brn1 with Ycs4 or Ycg1, respectively (Fig. 4a). This suggests that the two HEAT-repeat subunits might not directly interact with each other, but are instead tethered by their simultaneous binding to the kleisin subunit. This conclusion is consistent with the fact that the two HEAT-repeat subunits do not (Supplementary Fig. 6a) or only with very low efficiency[8] co-purify in the absence of the kleisin protein.

Notably, almost all cross-links with Ycg1 residues clustered within a small region of Brn1 (residues 409–573; Fig. 4a and b). This region of the kleisin subunit might

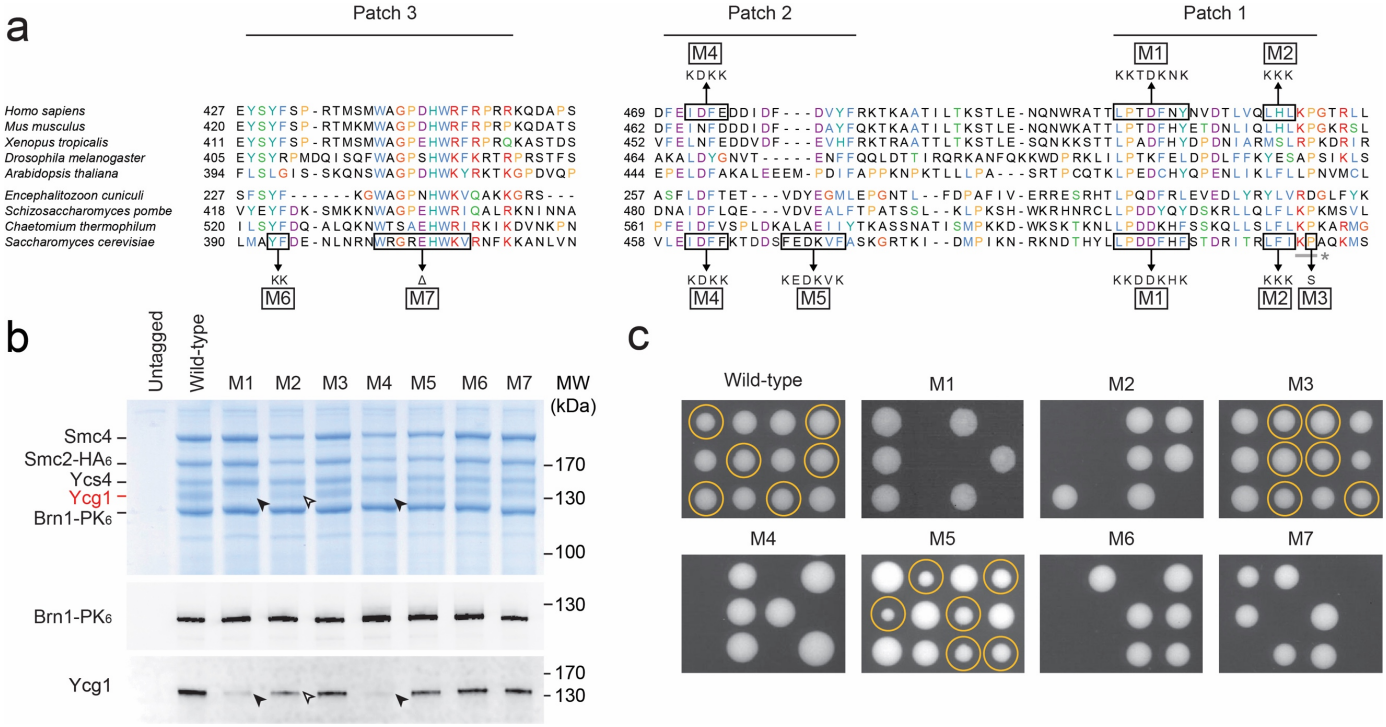

Figure 5 A conserved region within the Brn1 kleisin subunit for Ycg1 binding. (**a**) Multi-sequence alignment of the Ycg1-binding region of *S. cerevisiae* Brn1 with homologous γ-kleisins identifies three patches of conserved amino acid residues. Boxed residues were mutated to the indicated sequences in mutants M1-M7. Two residues mutated in *brn1-60* are indicated by a grey bar (*). (**b**) Co-immunoprecipitation of condensin subunits with the Brn1-PK$_6$ proteins from yeast cell extracts (strains C3632, C3665, C3651, C3641, C3635, C3658, C3649, C3634) was analyzed by Coomassie staining and western blotting with antibodies against Ycg1 or the PK epitope on Brn1. The identities of the Coomassie-stained bands were verified by mass spectrometry. Loss or reduction of Ycg1 binding in mutants M1, M4, and M2 is indicated by closed or open arrowheads, respectively. (**c**) Tetrad dissection analysis of diploid cells from **b** at 30°C on rich media. Circles indicate kanamycin-resistant colonies linked to the wild-type or mutant *BRN1-PK$_6$* alleles. Panels **b** and **c** show one representative experiment of $n = 3$ biological replicates.

therefore form a distinct binding domain for Ycg1. To test this notion, we expressed in budding yeast a series of Brn1 versions truncated either from the N or the C terminus and assayed which constructs bound endogenous Ycg1 (Supplementary Fig. 6b). Only Brn1 constructs that included the region between residues 439 and 531 co-purified Ycg1. This region was also sufficient for forming a stable complex with Ycg1 when expressed in yeast (Fig. 4c) or when recombinantly produced as an even shorter version (residues 458–531) in insect cells (Supplementary Fig. 6c). Similarly, the homologous region of the *Ct* Brn1 protein (residues 562–633) formed a stable complex with *Ct* Ycg1$_{\Delta C}$ (Fig. 4d). A small domain of ~70 amino acids within condensin's kleisin subunit is therefore sufficient for binding Ycg1.

Most cross-links with Ycs4 were located within a region N-terminal of the Ycg1-interacting domain (residues 232–450; Fig. 4a and 4b). When we tested co-purification of Ycs4 with truncated versions of Brn1 from yeast cell extracts under low salt conditions, we observed co-purification of Ycs4 with Brn1 fragments that contained the region between residues 224 and 340. The levels of Ycs4 that co-purified notably increased and co-purification was now detectable even under high salt conditions when we extended this region to residues 110–438 (Supplementary Fig. 6b). This region was indeed sufficient for Ycs4 binding (Fig. 4c). Moreover, the analogous region of the *Ct* Brn1 protein (residues 225–583)

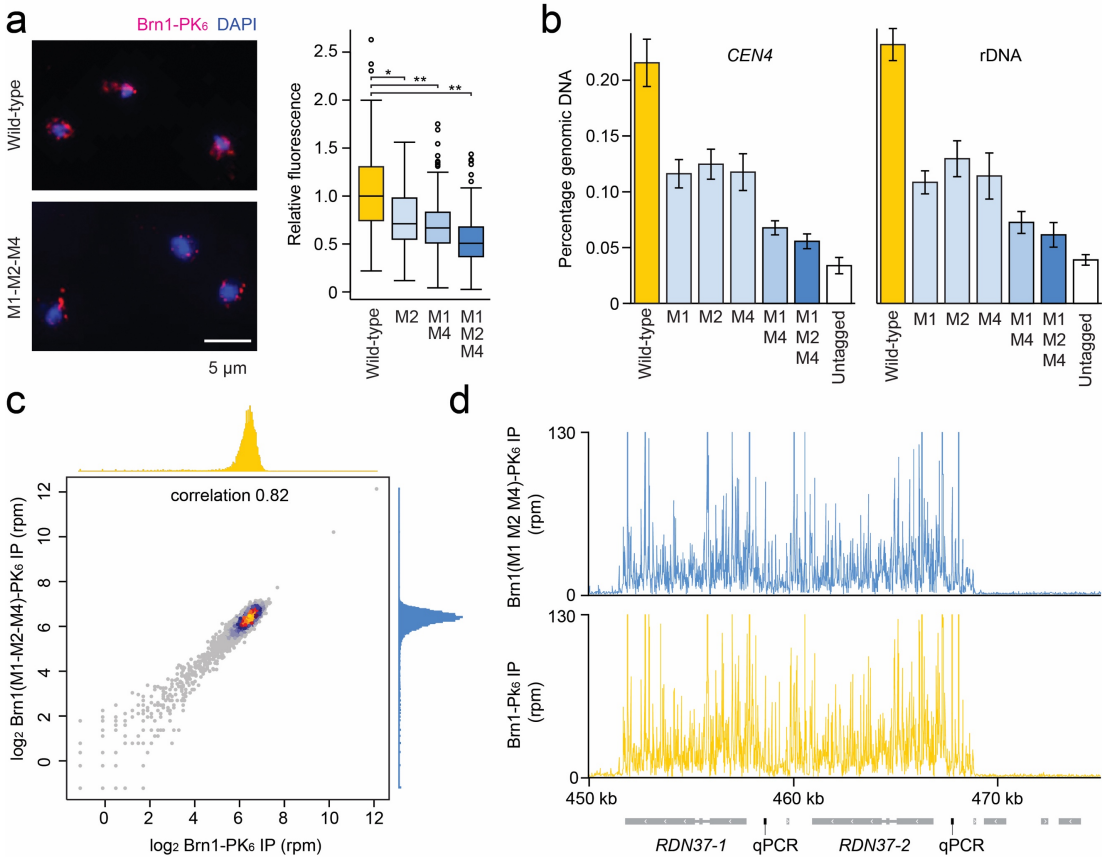

Figure 6 The Ycg1 subunit is essential for condensin recruitment onto yeast chromosomes. (**a**) Chromosome spreads prepared from asynchronous diploid yeast cells (C3632, C3651, C3856, C3857) were probed with anti-PK antibody (red) and stained with 4',6-diamidino-2-phenylindole (DAPI; blue). Brn1-PK$_6$ signals were quantified in 200 nuclei from $n = 2$ independent experiments. Horizontal lines define the median, boxes define the 25th and 75th percentiles, whiskers define the 10th and 90th percentiles. * $P = 8.1\times10^{-10}$; ** $P < 2.2\times10^{-16}$ by one-sided Wilcoxon–Mann–Whitney test. (**b**) ChIP-qPCR in asynchronous cells of diploid strains expressing wild-type (C3632), single mutants (C3665, C3651, C3635), or mutant combinations (C3856, C3857) of Brn1-PK$_6$ at the centromere of chromosome IV (*CEN4*) and the rDNA locus (5' UTR of *RDN37*). Data represent mean values of $n = 4$ ChIP experiments and two technical replicates per experiment ± s. d. (**c**) Scatter plot representing sequence coverage of ChIP-seq reads from yeast cells expressing wild-type Brn1-PK$_6$ (strain C3632, x-axis) and the Brn1 (M1 M2 M4)-PK$_6$ mutant (strain C3857, y-axis). Each point represents at 1,000 bp window of the budding yeast genome. (**d**) Sequence reads (reads per million, rpm) of wild-type and mutant Brn1-PK$_6$ cells from **c** at the rDNA locus on chromosome XII are displayed on a linear scale. The region used for qPCR analysis in **b** is indicated. Note that in **c** and **d**, sequence reads were normalized to the total number of reads for each sample individually to measure Brn1 positions independent of the absolute efficiency of Brn1 immunoprecipitation.

formed a stable complex with *Ct* Ycs4 when co-expressed in insect cells (Fig. 4e). We conclude that distinct binding domains exist within the central region of the condensin kleisin subunit for the recruitment of each HEAT-repeat subunit.

Functional condensin complexes require the Ycg1 subunit

Since the mapping experiments identified a distinct domain within Brn1 for binding to Ycg1, we reasoned that it should be possible to prevent incorporation of Ycg1 into condensin complexes by introducing specific mutations within this domain. Using alignments of γ-kleisin protein sequences from evolutionary distant species, we identified two patches of conserved residues in the Ycg1 binding domain (patches 1 and 2; Fig. 5a). We generated diploid budding yeast strains in which we introduced into one of the two endogenous *BRN1* alleles point mutations of hydrophobic residues located within patch 1 or 2, as well as a pair of point mutations or a short deletion of residues within a third conserved patch located just N-terminal of the Ycg1 binding domain (patch 3; Fig. 5a and Supplementary Table 4). Even though all Brn1 mutant versions were expressed at the same levels as the wild-type protein (Supplementary Fig. 7a), co-immunoprecipitation of Ycg1 with Brn1 mutant M2 or mutants M1 and M4 was reduced or completely abolished, respectively (Fig. 5b). None of the mutations affected co-purification of the other three condensin subunits (Fig. 5b and Supplementary Fig. 7b).

To test whether condensin complexes that cannot incorporate Ycg1 are functional, we induced meiosis in the diploid strains and dissected the four haploid progeny spores. Tetrad analysis demonstrated that Brn1 mutants M1, M2, and M4 failed to support growth at 30°C when present as the only source of Brn1 in yeast strains that expressed in addition HA_6-tagged Smc2 (Fig. 5c). In the absence of a tag on Smc2, mutants M1 and M4 were able to sustain cell growth at 25°C but not at 37°C. We used these two mutants to test whether the observed growth defects were due to defects in chromosome segregation that result from condensin inactivation[40,41]. Following release from a G1 phase arrest, we monitored mitotic chromosome segregation at 37°C of cells that express wild-type or mutant Brn1 by following the fluorescently marked arm of chromosome V using live cell microscopy (Supplementary Fig. 7c)[25]. Remarkably, 75% of Brn1 wild-type cells, but only 28% or 21% of Brn1 mutant M1 or M4 cells, respectively, had successfully segregated the marked sister chromatids into opposite daughter cells within 165 min after release from G1 phase. The failure to segregate

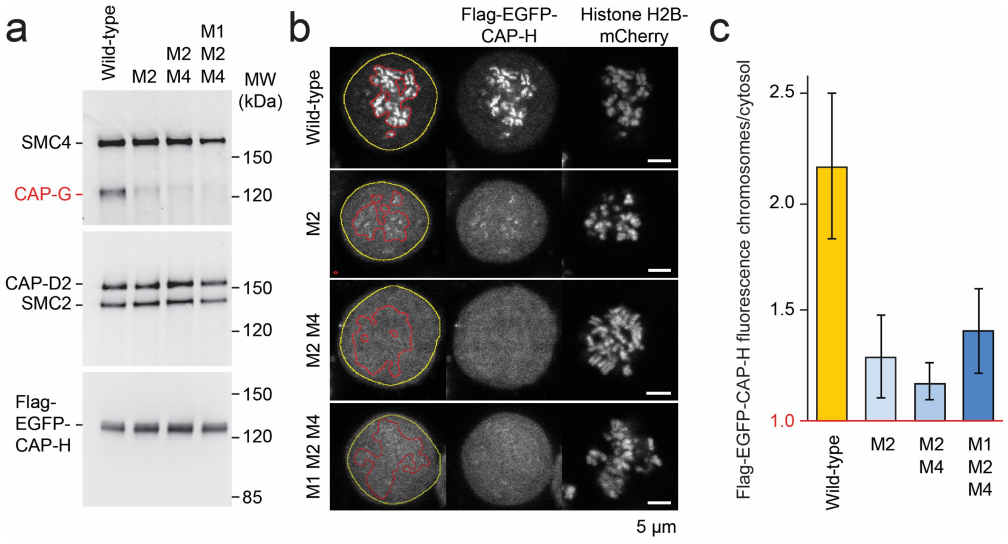

Figure 7 The CAP-G HEAT-repeat subunit is required for condensin binding to human chromosomes. (**a**) The indicated Flag-EGFP-CAPH proteins were immunoprecipitated from lysates of transiently transfected HEK 293 cells and co-precipitation of the other condensin subunits was probed by western blotting. One representative experiment of $n = 2$ biological replicates is shown. (**b**) Flag-EGFP-CAPH proteins were transiently expressed in nocodazole-arrested HeLa cells expressing histone H2B-mCherry. Cells (yellow lines) and chromosomes (red lines) were segmented using total EGFP or mCherry signals, respectively, and mean EGFP intensities were measured in chromosome and cytoplasmic regions. (**c**) Ratios between chromosomal and cytoplasmic EGFP mean intensities were calculated from one representative experiment of three biological replicates and plotted ± s. d. (n = 39-92 cells).

sister chromatids was not due to a delay in anaphase onset, as judged from FACScan profiles (Supplementary Fig. 7c) and monitoring mitotic spindle dynamics (Jutta Metz, unpublished data). We conclude that yeast condensin complexes that are deficient in recruiting Ycg1 are unable to support proper chromosome segregation and cell division. Interestingly, mutations within patch 3 adjacent (M6 and M7) abolished condensin function (Fig. 5c) without notably affecting Ycg1 or Ycs4 binding (Fig. 5b), suggesting that this patch has an essential function other than recruiting the HEAT-repeat subunits.

Recruitment to chromosomes by the HEAT-repeat subunits

The ability to generate 'tetrameric' condensin complexes enabled us to dissect the role of the Ycg1 HEAT-repeat subunit for condensin function *in vivo*. We first measured the protein levels associated with chromosomes of wild-type and mutant versions of Brn1 that had either reduced affinity to Ycg1 (M2) or were unable to bind Ycg1 (M1 M4 double or M1 M2 M4 triple mutants) by probing chromosome spreads from diploid yeast cells against the PK_6 epitope on Brn1 (Fig. 6a). The amounts of condensin on chromosomes were markedly reduced in the three mutants. To further quantify the reduction in condensin binding to chromosomes, we determined the levels of condensin at two different chromosomal binding sites using chromatin immunoprecipitation and quantitative PCR (ChIP-qPCR). At both sites tested, the amount of DNA that co-immunoprecipitated with the Brn1 M1, M2, or M4 single mutants was reduced to less than half when compared to wild-type Brn1 (Fig. 6b). Association with chromosomes was even further reduced in Brn1 double or triple mutants.

To distinguish whether the decrease in condensin binding at these sites was due to the repositioning of condensin from its usual binding regions to other chromosomal locations or due to a global reduction in chromosome association, we mapped the positions of the Brn1 triple mutant by ChIP-seq and compared them to the positions of wild-type Brn1 genome-wide (Fig. 6c) and at ribosomal RNA genes, transfer RNA genes, centromeres, and RNA pol II-transcribed genes (Fig. 6d and Supplementary Fig. 7d). The fact that we detected no obvious differences between the distributions of wild-type and triple mutant Brn1strongly suggests that Ycg1 is not involved in condensin targeting to specific chromosome sites, but is instead essential for the general recruitment of condensin onto chromosomes.

We next tested whether the conserved domain within the kleisin subunit that we identified for binding to the Ycg1 subunit fulfills the same function in mammalian condensin complexes. We transiently transfected human embryonic kidney (HEK) 293 cells with expression constructs for wild-type, single, double, or triple mutant versions of the CAP-H kleisin subunit of condensin I or the CAP-H2 kleisin subunit of condensin II fused to a Flag-EGFP epitope tag (Fig. 5a, Supplementary Fig. 8a, and Supplementary Table 4). We then immunoprecipitated Flag-tagged CAP-H or -H2 from whole cell extracts and probed for co-purification of the other four condensin subunits by western blotting. Remarkably, all three CAP-H mutants co-immunoprecipitated greatly reduced amounts of the Ycg1 homolog CAP-G without affecting the co-precipitation of the other three condensin I subunits (Fig. 7a). Similarly, the CAP-G2 subunit no longer co-immunoprecipitated with double and triple CAP-H2 mutants (Supplementary Fig. 8b).

We transiently expressed wild-type and mutant versions of Flag-EGFP-CAP-H in a HeLa cell line that stably expresses histone H2B tagged with mCherry [42]. All Flag-EGFP-CAP-H versions were produced at comparable levels, which were lower than the protein levels of endogenous CAP-H (Supplementary Fig. 8c). After arresting cells in mitosis with nocodazole, we measured the levels of Flag-EGFP-CAP-H associated with chromosomes (Fig. 7b). Strikingly, condensin I enrichment on chromosomes, which we define by the mean EGFP signal ratio of chromosomal to cytoplasmic regions, decreased from ~2.2 in cells expressing wild-type CAP-H to ~1.2 to 1.4 in cells expressing the three CAP-H mutants (Fig. 7c; note that a value of 1.0 corresponds to no condensin enrichment on chromosomes). Similarly, condensin II enrichment on chromosomes decreased from

~3.0 to ~1.1 and ~1.3 in the CAP-H2 double and triple mutants (Supplementary Fig. 8d and e). The decrease in chromosome binding was considerably less in the CAP-H2 single mutant, which did not notably affect CAP-G2 binding in the co-immunoprecipitation experiment (Supplementary Fig. 8b, d and e). We conclude that association with chromosomes of condensin I and II complexes that lack the CAP-G or -G2 subunit, respectively, is dramatically reduced in human cells, as is the association of condensin complexes that are devoid of Ycg1 in yeast cells. These findings suggest that the HEAT-repeat subunits play an essential and conserved role for the interaction of all condensin complexes with chromosomes *in vivo*, presumably by providing a DNA binding interface.

DNA binding by the non-SMC complex stimulates the SMC ATPase

Loading of the condensin-related cohesin complex onto chromosomes depends on ATP hydrolysis by its SMC subunits, which has been suggested to trigger transport of chromatin fibers into cohesin rings[43,44]. How such a mechanism would be activated in the vicinity of chromosomes is not known. We reasoned that DNA binding by the condensin non-SMC subcomplex might function as such a trigger. Consistent with previous reports[14], the presence of DNA had no apparent effect on the low ATPase activity of the Smc2–Smc4 dimer (~0.5 molecules ATP hydrolyzed per Smc2–Smc4 and min; Fig. 8a and b). Addition of the Brn1–Ycs4–Ycg1 non-SMC subcomplex enhanced the Smc2–Smc4 ATPase activity approximately 2-fold in the absence of DNA, similar to the activation of the Smc1–Smc3 ATPase activity by binding of the cohesin kleisin subunit Brn1[45], but more than 10-fold in the presence of DNA (Fig. 8b). The DNA-dependent stimulation of the Smc2–Smc4 ATPase activity was due to the binding of the non-SMC subcomplex to the Smc2–Smc4 head domains, since we observed no stimulation by DNA when we used a non-SMC subcomplex containing a version of Brn1 that lacks the Smc2–Smc4 interaction motives ($Brn1_{\Delta NC}$; Fig. 1e and 8b). To rule out that the increase in activity was due to a contaminating ATPase in the non-SMC subcomplex preparation, we repeated the assay with an Smc2–Smc4 dimer that contained point mutations in each of the two Walker B ATP hydrolysis motives. As expected, we measured no DNA-dependent ATPase activity for the mutant Smc2–Smc4 dimer, even in the presence of the non-SMC subcomplex (Fig. 8b). Our findings are in excellent agreement with the report that the 13S *Xenopus* condensin holocomplex displays a higher ATPase activity than the 8S SMC2–SMC4 subcomplex and increases ~2.5-fold in the presence of DNA[13].

Discussion

A DNA binding site formed by the HEAT-repeat subunits

How condensin complexes interact with their chromatin substrates has remained poorly understood. While the Smc2–Smc4 dimer has been previously reported to bind DNA, binding was considerably less pronounced when compared to condensin holocomplexes[13] and was readily disrupted by salt concentrations above 100 mM[14]. The C-terminal half of the Smc2 head[46] and the Smc2–Smc4 hinge domains[21] have been suggested to mediate direct protein-DNA interactions. While the former has now been shown to fold, together with the N-terminal half of the SMC head, into a canonical ATP-binding cassette ATPase domain devoid of any obvious DNA interaction motives[30-32,47], the latter bound much more efficiently to ssDNA than to dsDNA. Binding to ssDNA might be required for specific functions of condensin at a time when exposed single strands are present, for example during DNA damage repair or active transcription [23].

We find that the condensin non-SMC subcomplex, in contrast to the SMC hinge domain, binds to dsDNA with high selectivity over ssDNA (Fig. 2a and Supplementary Fig. 3 a-c). This is surprising, since DNA binding could previously not be detected with frog or fission yeast non-SMC subcomplexes[13,16]. The facts that binding of the budding yeast non-SMC subcomplex to different dsDNA substrates occurs at low micro-molar affinity, that it is reversible, and that it depends on a minimum DNA length (Fig. 1 and Supplementary Fig. 2) argue against the

possibility that association might be merely due to non-specific electrostatic interactions. These would also seem unlikely for a protein complex that is predicted to display a negative surface charge (*pI* = 4.9). Moreover, a non-SMC subcomplex from an evolutionary distant yeast species displays similar dsDNA binding properties (Fig. 3b).

Computational sequence analyses of the condensin non-SMC subunits failed to detect canonical DNA binding motives in addition to the HTH and WHD motives in the kleisin subunit, which, as we show, do not contribute to the DNA binding activity (Fig. 1e and f). This suggests that DNA binding might instead be achieved by the two HEAT-repeat subunits. Intriguingly, a recent crystal structure of the AlkD glycosylase in complex with DNA revealed the binding of a 12 bp dsDNA helix along the concave surface of six tandem HEAT repeats[48]. Since the AlkD HEAT-repeat motives mainly contact the phosphate backbone of the DNA helix, binding is thought to be largely sequence-independent[48]. Interestingly, the non-SMC subcomplex binds dsDNA with a similar affinity as AlkD and also shows no sequence specificity (Fig. 1d and 2a). Condensin's HEAT-repeat subunits might therefore bind DNA helices in a manner analogous to AlkD.

Condensin holocomplexes have been previously found to associate with nucleosomes assembled in *Xenopus* egg extracts[13]. Interactions with histones might be mediated via binding of a phosphorylated N-terminal extension of the γ-kleisin subunit to histones H2A or H2A.Z in condensin I-type complexes[27] or via binding of the HEAT-repeat subunits to histone H4 tails mono-methylated at lysine 20 in condensin II complexes[28]. In contrast, we cannot detect evidence for an interaction between budding yeast condensin and nucleosomes *in vitro* (Fig. 2b) or *in vivo* (Fig. 2c and Supplementary Fig. 3e). This is consistent with the lack of the N-terminal extension in the γ-kleisin subunits of many yeast species, including *S. cerevisiae* (Supplementary Fig. 7). It is therefore unlikely that the interaction with nucleosomes serves as the universal basis for chromatin substrate recognition by condensin complexes. We propose that the newly discovered DNA binding domain formed by the HEAT-repeat subunits fulfills this function instead.

Geometry of the non-SMC subcomplex

Cross-linking mass-spectrometry and co-purification analyses suggest that the central region of the *S. cerevisiae* condensin kleisin subunit functions as a linker molecule for binding Ycs4 and Ycg1 by distinct domains within its N- or C-terminal halves, respectively (Fig. 8c). The interaction domain for the Ycg1 subunit is confined to a short region of less than 100 residues. The findings that this Brn1 domain forms stable complexes with Ycg1 (Fig. 4 and Supplementary Fig. 6c), that mutation of a few residues of two conserved patches within this domain abolishes binding to Ycg1 (Fig. 5a and b), and that overexpression of Ycg1 rescues the temperature-sensitive phenotype of the *brn1-60* mutant[49], which contains two amino acid substitutions within patch 1 (Fig. 5a), suggest that this domain is both necessary and sufficient for Ycg1 recruitment to condensin complexes. The Brn1 region that is required for stable binding to Ycs4 is, in contrast, considerably larger (Fig. 4b). We attempted to also disrupt Ycs4 binding to Brn1 by mutating conserved stretches within this region. However, mutation of several conserved residues only reduced, but did not abolish, Ycs4 binding (I.P., unpublished data).

The overall arrangement of binding domains for the two HEAT-repeat subunits is identical in *S. cerevisiae*, *C. thermophilum* and human β- and γ-kleisin subunits (Fig. 4-6, Supplementary Fig. 8, and ref. 8), suggesting that the architecture of eukaryotic non-SMC subcomplexes has been strictly conserved. Interestingly, prokaryotic condensin kleisin subunits associate with pairs of WHD proteins that have no resemblance to the eukaryotic HEAT-repeat subunits [30]. The role of the HEAT-repeat subunits in binding to DNA (see above) must therefore have been acquired by eukaryotic condensins after their evolutionary divergence from a common SMC precursor complex.

Linkage of the Ycs4 and Ycg1 subunits by Brn1 notably enhances their DNA binding activity (Fig. 3b). Since addition of either of the two subunits changes the

electrophoretic mobility of dsDNA substrates, it is possible that separate DNA binding sites exist in the two subunits and that the higher affinity of the complete non-SMC subcomplex can be explained by the multiplication of their binding affinities. Alternatively, the two HEAT-repeat subunits might form a combined DNA binding site. It remains to be tested whether the kleisin subunit in this context merely acts as a scaffold to bring these two subunits into proximity or whether it has an active role in promoting the formation of the DNA binding site(s). The cooperative action of Ycs4 and Ycg1 is presumably essential for condensin function, since *in vivo* binding to chromosomes of condensin complexes that only contain the Ycs4, CAP-D2, or CAP-D3 HEAT-repeat subunit is strongly reduced (Fig. 6a and b, 7b and c, and Supplementary Fig. 8d and e) and mutations in either HEAT-repeat protein reduce the levels of chromosome-associated Smc4 in yeast[40].

A multi-step model for loading condensin onto chromosomes

A central feature of SMC protein complexes like cohesin or condensin is the entrapment of chromosomal DNA within their large ring structures[25,50]. How chromatin fibers end up within these protein rings is, however, not understood. For cohesin, it has been suggested that ATP hydrolysis by the Smc1–Smc3 head domains drives the temporary opening of the ring[43,44], presumably at Smc1–Smc3 hinge interface[51], to allow the entry of chromosomes. Whether condensin might use a similar mechanism is not known. The observation that Smc2 proteins that are either defective in ATP hydrolysis can still associate with mitotic chromosomes[52] argue against this possibility. Yet, the identification of a direct DNA binding site in the condensin non-SMC subcomplex can explain how condensin is, in principle, able to still bind to chromosomes even without encircling them. A direct protein-DNA interaction could also be the reason for the requirement of high salt conditions to efficiently release condensin (but not cohesin) from linearized minichromosomes *in vitro*[25].

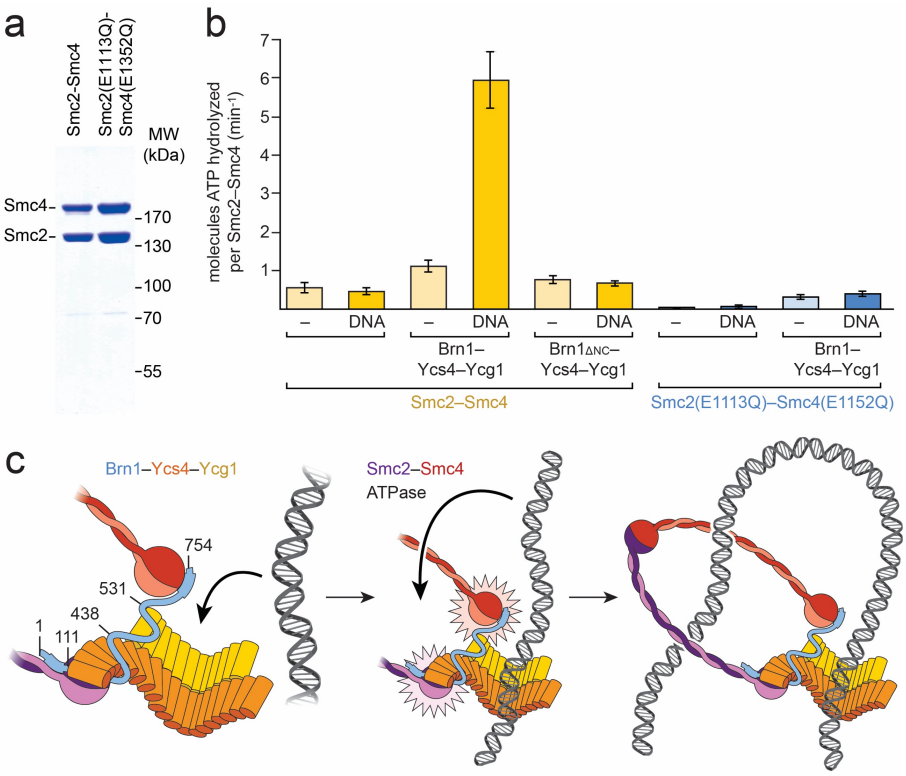

Figure 8 DNA binding by the non-SMC subcomplex activates the Smc2–Smc4 ATPases. (**a**) Wild-type and Walker B mutant Smc2–Smc4 complexes were analyzed by SDS PAGE and Coomassie staining. (**b**) ATP (1.25 mM) hydrolysis rates of *S. cerevisiae* wild-type or hydrolysis-defective Smc2–Smc4 dimers (0.5 μM) were measured in the presence or absence of the Brn1–Ycs4–Ycg1 subcomplex (1.5 μM), the Brn1$_{\Delta NC}$–Ycs4–Ycg1 subcomplex (1.5 μM) lacking the Smc2–Smc4 interaction motives, and/or 6.5 kb linearized plasmid DNA (10 nM). Columns and error bars indicate mean and s. d. of n = 3 technical replicates. (**c**) Multi-step model for the topological loading of condensin onto chromosomes. Binding of duplex DNA to the HEAT-repeat subunits (left) activates of the Smc2–Smc4 ATPase activity (middle), which triggers the transfer of DNA into the condensin ring (right). Numbers indicate the binding regions for Ycs4 and Ycg1 in the *S. cerevisiae* Brn1 kleisin subunit.

Binding to DNA via its non-SMC subunits might serve as the first step in the condensin loading mechanism (Fig. 8c). This interaction consequently activates the Smc2–Smc4 ATPases (Fig. 8b). We

hypothesize that activation of the ATPase cycle, in a second step, triggers the topological loading of condensin rings onto the tethered chromatin fiber (Fig. 8c), potentially by inducing a temporary opening of the ring for the passage of DNA in an analogous manner to what has been proposed for cohesin. The role of the HEAT-repeat subunits in the tethering step might be taken over by a separate Scc2–Scc4 protein complex during the loading of cohesin onto chromosomes. Interestingly, Scc2 and Scc4 were predicted to contain α-helical HEAT or tetratricopeptide (TPR) repeats, respectively, and were recently shown to stimulate cohesin's ATPase activity for efficient chromosome loading *in vitro* [53]. How the HEAT-repeat subunits precisely contact DNA, how this leads to activation of the SMC ATPases, and how these steps are regulated by posttranslational modifications are important questions for future research.

Accession Codes

ChIP-seq data were deposited at the NCBI's Gene Expression Omnibus portal under GEO Series accession number GSE55948.

Acknowledgements

We are grateful to J. Metz, M. Cohen, V. Rybin, M. Saravanan, C. Tischer for assistance with yeast experiments, biophysical assays, nucleosome preparation, and image segmentation, to Y. Frosi for suggesting the mutant analysis in human cells, and to S. Amlacher and E. Hurt (University of Heidelberg) for providing *C. thermophilum* cDNA and condensin sequences. We thank I. Berger for extensive advice and training in the multi-bac technology, the EMBL Advanced Light Microscopy, Genomics, and Proteomics Core Facilities for technical support. We thank V. Benes and B. Baying for discussion, technical advice, and help with the preparation of genomic libraries and sequencing. We thank F. Baudin, J. Ellenberg, D. Gilmour, F. Melchior, S. Milles, A. Musacchio, C. Müller, and members of the Haering lab for discussion and advice. This work was supported by funding from EMBL and the German Research Foundation (DFG) grant HA 5853/2-1 (C.H.H.). A.O. was supported by postdoctoral fellowships from the Alexander von Humboldt foundation and Marie Curie Actions.

Author Contributions

I.P., A.R., A.O., M.W. and C.H.H. designed and performed the experiments, I.P., A.O. and M.B. analyzed the cross-linking mass spectrometry experiments, I.P. and V.P. performed bioinformatics analysis of generated and published ChIP-seq data, I.P. and C.H.H. wrote the manuscript with contributions from all authors.

References

1. Hirano, T. Condensins: universal organizers of chromosomes with diverse functions. *Genes Dev* **26,** 1659–1678 (2012).
2. Piazza, I., Haering, C. H. & Rutkowska, A. Condensin: crafting the chromosome landscape. *Chromosoma* (2013). doi:10.1007/s00412-013-0405-1
3. Aragón, L., Martinez-Perez, E. & Merkenschlager, M. Condensin, cohesin and the control of chromatin states. *Curr Opin Genet Dev* (2013). doi:10.1016/j.gde.2012.11.004
4. Wood, A. J., Severson, A. F. & Meyer, B. J. Condensin and cohesin complexity: the expanding repertoire of functions. *Nat Rev Genet* **11,** 391–404 (2010).
5. Hirano, T., Kobayashi, R. & Hirano, M. Condensins, chromosome condensation protein complexes containing XCAP-C, XCAP-E and a Xenopus homolog of the Drosophila Barren protein. *Cell* **89,** 511–521 (1997).
6. Anderson, D. E., Losada, A., Erickson, H. P. & Hirano, T. Condensin and cohesin display different arm conformations with characteristic hinge angles. *J Cell Biol* **156,** 419–424 (2002).
7. Schleiffer, A. *et al.* Kleisins: a superfamily of bacterial and eukaryotic SMC protein partners. *Mol Cell* **11,** 571–575 (2003).
8. Onn, I., Aono, N., Hirano, M. & Hirano, T. Reconstitution and subunit geometry of human condensin complexes. *EMBO J* **26,** 1024–1034 (2007).
9. Neuwald, A. F. & Hirano, T. HEAT repeats associated with condensins, cohesins, and other complexes involved in chromosome-related functions. *Genome Res* **10,** 1445–1452 (2000).
10. Ono, T., Fang, Y., Spector, D. L. & Hirano, T. Spatial and temporal regulation of Condensins I and II in mitotic chromosome assembly in human cells. *Mol Biol Cell* **15,** 3296–3308 (2004).
11. Kimura, K. & Hirano, T. ATP-dependent positive supercoiling of DNA by 13S condensin: a biochemical implication for chromosome condensation. *Cell* **90,** 625–634 (1997).

12. Kimura, K., Rybenkov, V. V., Crisona, N. J., Hirano, T. & Cozzarelli, N. R. 13S condensin actively reconfigures DNA by introducing global positive writhe: implications for chromosome condensation. *Cell* **98,** 239–248 (1999).

13. Kimura, K. & Hirano, T. Dual roles of the 11S regulatory subcomplex in condensin functions. *Proc Natl Acad Sci USA* **97,** 11972–11977 (2000).

14. Stray, J. E. & Lindsley, J. E. Biochemical analysis of the yeast condensin Smc2/4 complex: an ATPase that promotes knotting of circular DNA. *J Biol Chem* **278,** 26238–26248 (2003).

15. Stray, J. E., Crisona, N. J., Belotserkovskii, B. P., Lindsley, J. E. & Cozzarelli, N. R. The Saccharomyces cerevisiae Smc2/4 condensin compacts DNA into (+) chiral structures without net supercoiling. *J Biol Chem* **280,** 34723–34734 (2005).

16. Sakai, A., Hizume, K., Sutani, T., Takeyasu, K. & Yanagida, M. Condensin but not cohesin SMC heterodimer induces DNA reannealing through protein-protein assembly. *EMBO J* **22,** 2764–2775 (2003).

17. Chiu, A., Revenkova, E. & Jessberger, R. DNA interaction and dimerization of eukaryotic SMC hinge domains. *J Biol Chem* **279,** 26233–26242 (2004).

18. Griese, J. J. & Hopfner, K.-P. Structure and DNA-binding activity of the Pyrococcus furiosus SMC protein hinge domain. *Proteins* **79,** 558–568 (2011).

19. Hirano, M. & Hirano, T. Hinge-mediated dimerization of SMC protein is essential for its dynamic interaction with DNA. *EMBO J* **21,** 5733–5744 (2002).

20. Hirano, M. & Hirano, T. Opening closed arms: long-distance activation of SMC ATPase by hinge-DNA interactions. *Mol Cell* **21,** 175–186 (2006).

21. Griese, J. J., Witte, G. & Hopfner, K.-P. Structure and DNA binding activity of the mouse condensin hinge domain highlight common and diverse features of SMC proteins. *Nucleic Acids Res* **38,** 3454–3465 (2010).

22. Yoshimura, S. H. *et al.* Condensin architecture and interaction with DNA: regulatory non-SMC subunits bind to the head of SMC heterodimer. *Curr Biol* **12,** 508–513 (2002).

23. Akai, Y. *et al.* Opposing role of condensin hinge against replication protein A in mitosis and interphase through promoting DNA annealing. *Open Biology* **1,** 110023–110023 (2011).

24. Sutani, T. & Yanagida, M. DNA renaturation activity of the SMC complex implicated in chromosome condensation. *Nature* **388,** 798–801 (1997).

25. Cuylen, S., Metz, J. & Haering, C. H. Condensin structures chromosomal DNA through topological links. *Nat Struct Mol Biol* **18,** 894–901 (2011).

26. Haering, C. H., Farcas, A.-M., Arumugam, P., Metson, J. & Nasmyth, K. The cohesin ring concatenates sister DNA molecules. *Nature* **454,** 297–301 (2008).

27. Tada, K., Susumu, H., Sakuno, T. & Watanabe, Y. Condensin association with histone H2A shapes mitotic chromosomes. *Nature* **474,** 477–483 (2011).

28. Liu, W. *et al.* PHF8 mediates histone H4 lysine 20 demethylation events involved in cell cycle progression. *Nature* **466,** 508–512 (2010).

29. Gajiwala, K. S. & Burley, S. K. Winged helix proteins. *Curr Opin Struct Biol* **10,** 110–116 (2000).

30. Bürmann, F. *et al.* An asymmetric SMC-kleisin bridge in prokaryotic condensin. *Nat Struct Mol Biol* **20,** 371–379 (2013).

31. Haering, C. H. *et al.* Structure and stability of cohesin's Smc1-kleisin interaction. *Mol Cell* **15,** 951–964 (2004).

32. Woo, J.-S. *et al.* Structural studies of a bacterial condensin complex reveal ATP-dependent disruption of intersubunit interactions. *Cell* **136,** 85–96 (2009).

33. Lowary, P. T. & Widom, J. New DNA sequence rules for high affinity binding to histone octamer and sequence-directed nucleosome positioning. *J Mol Biol* **276,** 19–42 (1998).

34. Verzijlbergen, K. F. *et al.* Shugoshin biases chromosomes for biorientation through condensin recruitment to the pericentromere. *Elife* **3,** e01374 (2014).

35. Mavrich, T. N. *et al.* A barrier nucleosome model for statistical positioning of nucleosomes throughout the yeast genome. *Genome Res* **18,** 1073–1083 (2008).

36. Albert, I. *et al.* Translational and rotational settings of H2A.Z nucleosomes across the Saccharomyces cerevisiae genome. *Nature* **446,** 572–576 (2007).

37. Amlacher, S. *et al.* Insight into structure and assembly of the nuclear pore complex by utilizing the genome of a eukaryotic thermophile. *Cell* **146,** 277–289 (2011).

38. Leitner, A. *et al.* Probing native protein structures by chemical cross-linking, mass spectrometry, and bioinformatics. *Mol Cell Proteomics* **9,** 1634–1649 (2010).

39. Leitner, A. *et al.* Expanding the chemical cross-linking toolbox by the use of multiple proteases and enrichment by size exclusion chromatography. *Mol Cell Proteomics* **11,** M111.014126 (2012).

40. Lavoie, B. D., Hogan, E. & Koshland, D. In vivo dissection of the chromosome condensation machinery: reversibility of condensation distinguishes contributions of condensin and cohesin. *J Cell Biol* **156,** 805–815 (2002).

41. Cuylen, S., Metz, J., Hruby, A. & Haering, C. H. Entrapment of Chromosomes by Condensin Rings Prevents Their Breakage during Cytokinesis. *Dev Cell* **27,** 469–478 (2013).

42. Neumann, B. *et al.* Phenotypic profiling of the human genome by time-lapse microscopy reveals cell division genes. *Nature* **464,** 721–727 (2010).

43. Arumugam, P. *et al.* ATP hydrolysis is required for cohesin's association with chromosomes. *Curr Biol* **13,** 1941–1953 (2003).

44. Weitzer, S., Lehane, C. & Uhlmann, F. A model for ATP hydrolysis-dependent binding of cohesin to DNA. *Curr Biol* **13,** 1930–1940 (2003).

45. Arumugam, P., Nishino, T., Haering, C. H., Gruber, S. & Nasmyth, K. Cohesin's ATPase activity is stimulated by the C-terminal Winged-Helix domain of its kleisin subunit. *Curr Biol* **16,** 1998–2008 (2006).

46. Akhmedov, A. T. *et al.* Structural maintenance of chromosomes protein C-terminal domains bind preferentially to DNA with secondary structure. *J Biol Chem* **273,** 24088–24094 (1998).

47. Lammens, A., Schele, A. & Hopfner, K.-P. Structural Biochemistry of ATP-Driven Dimerization and DNA-Stimulated Activation of SMC ATPases. *Current Biology* **14,** 1778–1782 (2004).

48. Rubinson, E. H., Gowda, A. S. P., Spratt, T. E., Gold, B. & Eichman, B. F. An unprecedented nucleic acid capture mechanism for excision of DNA damage. *Nature* **468,** 406–411 (2010).

49. Ouspenski, I. I., Cabello, O. A. & Brinkley, B. R. Chromosome condensation factor Brn1p is required for chromatid separation in mitosis. *Mol Biol Cell* **11,** 1305–1313 (2000).

50. Ivanov, D. & Nasmyth, K. A topological interaction between cohesin rings and a circular minichromosome. *Cell* **122,** 849–860 (2005).

51. Gruber, S. *et al.* Evidence that loading of cohesin onto chromosomes involves opening of its SMC hinge. *Cell* **127,** 523–537 (2006).

52. Hudson, D. F. *et al.* Molecular and genetic analysis of condensin function in vertebrate cells. *Mol Biol Cell* **19,** 3070–3079 (2008).

53. Murayama, Y. & Uhlmann, F. Biochemical reconstitution of topological DNA binding by the cohesin ring. *Nature* (2013). doi:10.1038/nature12867

Online Methods

Protein expression and purification

Non-SMC subunits and subcomplexes (Supplementary Table 1) were cloned into a single bacmid following the MultiBac protocol (Fitzgerald 2006). Due to ambiguities of the start codon annotation, the N-terminal 26 residues of *Ct* Ycg1 and *Ct* Ycs4 were removed. The C-terminal tail of *Ct* Ycg1 was removed, since it was predicted to be unstructured. Proteins were (co-)expressed in Sf21 cells cultured in Sf-900 III SFM serum free medium (Invitrogen). About 2×10^9 Sf21 cells were lysed using a tissue grinder in lysis buffer (25 mM TRIS-HCl pH 8.0, 250 mM NaCl, 10 mM imidazole, 0.1% NP40) containing 50 µM leupeptin (Serva), 5 µM pepstatin (Serva), 1×Pefabloc SC (Serva), 30 µg/µL DNase I (Roche), 5 mM β-mercaptoethanol at 4°C. Following centrifugation at 45,000×g for 30 min at 4°C, cleared lysates were loaded onto Ni-NTA Fast Flow (GE Healthcare) and/or Strep-Tactin Superflow (IBA) columns. Columns were washed extensively with wash buffer (25 mM TRIS-HCl pH 8.0, 150-300 mM NaCl, 5 mM β-mercaptoethanol, plus 30 mM imidazole for Ni-NTA). Proteins were eluted with 5 column volumes (CVs) of elution buffer (25 mM TRIS-HCl pH 8.0, 150 mM NaCl, plus 300 mM imidazole for Ni-NTA or 3 mM D-desthiobiotin for Strep-Tactin). Eluates were loaded onto a Source 15Q 4.6/100 PE anion exchange column (GE Healthcare) pre-equilibrated with 20 mM HEPES-KOH pH 8.0, 150 mM NaCl, 0.4 mM TCEP. The column was washed with 10 CVs of the same buffer and eluted by increasing the NaCl concentration to 1 M in a gradient of 25 ml. Peak fractions were concentrated by ultrafiltration (Vivaspin 100,000 MWCO, Sartorius) and loaded onto a Superose 6 size-exclusion column (GE Healthcare) in 20 mM HEPES-KOH pH 8.0, 180 mM NaCl, 2% glycerol, 0.4 mM TCEP.

Recombinant nucleosomes were reconstituted by salt dialysis as described (Luger 1999, Saravanan 2012), using *S. cerevisiae* recombinant histone octamers and a 167 bp dsDNA fragment derived from the strong 601 positioning sequence (Lowary 1998).

Genes encoding the *S. cerevisiae* Smc2 and Smc4-His_6 hinge domains were cloned in the pET28 *E. coli* expression

vector. Expression was induced for 16 h at 18°C in the *E. coli* BL21-CodonPlus(DE3)-RIPL strain (Agilent) and purified after lysis by sonication via Ni-NTA as described above. Eluate fractions were dialyzed against 20 mM NaPi pH 7.2, 300 mM NaCl, 2 mM DTT and loaded onto a Superdex 200 26/60 gelfiltration column (GE Healthcare) equilibrated in 20 mM NaP_i pH 7.2, 1 mM EDTA, 300 mM NaCl, 1 mM NaN_3, 2 mM DTT.

Smc2-His_6 and Smc4-StrepII were co-expressed from the pGAL10 or pGAL1 promoter, respectively, on a 2μ-based plasmid in *S. cerevisiae*. Yeast cells were grown at 30°C in –TRP media containing 2% raffinose to early log phase and expression was induced for 12 h by addition of galactose to 2%. Cells were harvested and resuspended in lysis buffer (50 mM TRIS-HCl pH 7.5, 200 mM NaCl, 2 ×cOmplete EDTA-free protease inhibitor mix (Roche)), and broken by cryogenic lysis in a Freezer/Mill (Spex). Extracts were cleared centrifugation at 43,400×g and loaded onto 6 ml Ni-NTA Fast Flow after adjusting imidazole to 20 mM. Proteins were eluted in lysis buffer plus 300 mM imidazole and loaded onto 5 ml Strep-Tactin Superflow high capacity after addition of EDTA and DTT to 1 mM. Proteins were eluted in lysis buffer plus 10 mM desthiobiotin and loaded onto a Superose 6 size-exclusion column in 20 mM TRIS-HCl pH 7.5, 150 mM NaCl, 1 mM DTT. Wild-type and mutant Smc2–Smc4 dimers were concentrated to 1-3 mg/ml by ultrafiltration (Vivaspin 30,000 MWCO).

Electron microscopy

Protein samples were diluted to 0.02 μg/μl and applied onto custom made carbon-coated grids glow-discharged in air. Grids were stained with 2% uranyl acetate and air dried for 10 min before imaging in a Morgagni FEI TEM operated at 100 kV and equipped with an SIS MegaView CCD camera at 40,000× magnification.

DNA binding assays

Linear 6.5 kb dsDNA templates were prepared by SpeI digestion of a circular plasmid containing part of the rDNA repeat sequence (Cuylen 2011). 15-60 bp dsDNA substrates were generated by annealing complementary HPLC-purified oligonucleotides (IDT), one of which was labeled with 6-FAM at the 5' end (Supplementary Fig. 2b), at a final concentration of 20 μM in 10 mM HEPES-KOH pH 7.5, 125 mM NaCl, 5 mM $MgCl_2$. Successful annealing and purity of the oligonucleotides were confirmed by electrophoresis and size-exclusion chromatography.

Reaction mixtures for the EMSA experiments contained a final concentration of 9.5 pM of 6.5 kb dsDNA or 200 nM of DNA oligos and varying concentrations of non-SMC or Smc2–Smc4 hinge complexes in 50 mM HEPES-KOH pH 7.5, 650 mM NaCl, 35 mM $MgCl_2$, 5 mM β-mercaptoethanol in a volume of 50 μl. To test binding to recombinant nucleosomes, 4 μg histone octamers were dialyzed against 50 mM HEPES-KOH pH 7.5, 650 mM NaCl, 35 mM $MgCl_2$, 5 mM β-mercaptoethanol and an equimolar amount of 167-bp DNA. The resulting nucleosomes were incubated with varying concentrations of non-SMC complex in the same buffer conditions. DNA-protein complexes were resolved by electrophoresis at 4°C on 0.7% TAE-agarose gels (16 h at 3 V/cm) for the 6.5 kb dsDNA substrate, on 1.8% TBE-agarose gels (5 h at 8 V/cm) for 15-60 bp dsDNA and 30 bp ssDNA substrates, or on 1.6 % TBE-agarose gels (overnight at 3 V/cm) for Nuc-167. Nuc-167 and 6.5 kb dsDNA was detected by post-run ethidium bromide staining, 6-FAM-labeled oligonucleotides were visualized at λ_{em} = 520 nm using an FLA-7000 scanner (Fujifilm).

Fluorescence anisotropy experiments were carried out at 100 nM 6-FAM DNA and variable concentrations of protein (0.006–36 μM). Anisotropy readings were recorded after 30 min incubation of the binding reactions at room temperature in a microplate reader (BioTek) at λ_{ex} = 485 nm and λ_{em} = 525 nm.

Normalized fluorescence anisotropy ΔA was calculated using

$$\Delta A = (r_n - r_0) / (r_{max} - r_0)$$

where r_0 is the anisotropy without protein, r_{max} is the anisotropy at the highest protein concentration.

For estimating equilibrium dissociation constants (K_d), the normalized fluorescence anisotropy was plotted as a function of protein concentration and a curve was fit to the full quadratic expansion of the binding polynomial derived for the total concentrations of:

$$\Delta A = \frac{\Delta A_T}{2D_T}\left\{\left(E_T + D_T + Kd\right) - \sqrt{\left(E_T + D_T + Kd\right)^2 - 4E_T D_T}\right\}$$

where ΔA_T is the total anisotropy change after saturation of the curve, E_T is the total protein concentration at each point in the titration and D_T is the total DNA concentration. The DNA-protein binding constants were confirmed in two independent experiments performed with different batches of purified proteins.

Subunit mapping by cross-linking mass spectrometry

0.1-5 mM H12/D12 isotope labeled disuccimidyl suberate (Creative Molecules) were mixed with 50 ug of the non-SMC complex in 20 mM HEPES-KOH pH 8.0, 200 mM NaCl, 0.5 mM TCEP. Crosslinking reactions were incubated for 40 min at 24°C and quenched by addition of NH_4HCO_3 to 0.1 M for 10 min at 24°C. Cross-linked proteins were denatured in 4 M urea and 0.1% RapiGest (Waters), treated with 10 mM DTT for 30 min at 37°C, and with 15 mM iodoacetamide for 30 min in the dark. After dilution of the urea concentration to 1.5 M, protein was digested first using 0.5 µg Lys-C endoproteinase (Wako) for 4 h at 37°C and then 1 µg trypsin (Promega) overnight at 37°C. Trifluoroacetic acid (TFA) was added to 0.5% (v/v). Peptides were desalted using MicroSpin columns (Harvard Apparatus), dried, and reconstituted with 30% (v/v) acetonitrile in 0.1% (v/v) formic acid. Cross-linked peptides were enriched by size-exclusion chromatography on a Superdex Peptide PC 3.2/30 column (GE Healthcare) as described (Leitner 2012).

Between 2% and 10% of the size-exclusion fractions were loaded onto a BEH300 C18 (75 µm × 250 mm, 1.7 µm) nanoAcquity UPLC column (Waters) and stepwise eluted with a 3–85% (v/v) ACN in 0.1% (v/v) formic acid gradient connected online to an LTQ-Orbitrap Velos Pro mass spectrometer (Thermo). Data acquisition was performed using a TOP-20 strategy where survey ms scans (m/z range 375–1,600) were acquired in the Orbitrap (R = 30,000), and up to 20 of the most abundant ions per full scan were fragmented by collision-induced dissociation (normalized collision energy = 40, activation Q = 0.250) and analyzed in the LTQ. In order to focus the acquisition on larger cross-linked peptides, charge states 1, 2, and unknown were rejected. Dynamic exclusion was enabled with repeat count = 1, exclusion duration = 60 s, list size = 500, and mass window ±15 ppm. Ion target values were 1,000,000 (or 500 ms maximum fill time) for full scans and 10,000 (or 50 ms maximum fill time) for ms/ms scans. At least two technical replicates per sample were measured.

Raw files were converted to centroid mzXML using the MassMatrix file conversion tool (Xu 2008da) and then analyzed using xQuest (Rinner 2008) and xProphet (Walzthoeni 2012). The results were filtered using the following parameters: FDR = 0.05, min delta score = 0.95, MS1 tolerance window ±3 ppm. All selected cross-links were classified, and only high confidence linkages with an LD score > 20 (Supplementary Fig. 5b) observed in at least two independent experiments were considered.

Multi-sequence alignments

Sequence alignments were performed using the T-Coffee software package (Notredame 2000) and secondary structure predictions were obtained from the Phyre2 protein homolog-fold recognition server (Kelley 2009). Conserved residues were highlighted accordingly to the ClustalW color code (Thompson 1994).

Yeast experiments

All strains are derivatives of W303; detailed genotypes are listed in Supplementary Table 5. Segregation of chromosome V was monitored by FACScan and live cell microscopy as described (Cuylen 2011).

Input, unbound, and bound samples (10×) from yeast immunoprecipitation experiments were separated on 4-12% or 7% SDS PAGE and probed by western blotting against Protein A (1:5000, Sigma P1291), HA (1:15,000, abcam ab9110), myc (1:10,000, Gramsch CM-100), PK (1:1,000, AbD Serotec MCA1360), or a polyclonal antibody raised in rabbit against *S. cerevisiae* Ycg1 residues 1–524 (1:1,000, Eurogentec).

Condensin and purification from yeast extracts

Expression of truncated versions of Brn1 fused to a Protein A tag was induced from ectopic copy of the gene under the control of the galactose-inducible *GAL10* promoter on a centromeric plasmid by addition to the media of galactose to 2% for 4 h at 30°C. Extracts from ~50 mOD_{600} culture were prepared by glass bead lysis in 1 ml EBX buffer (50 mM HEPES-KOH pH 7.5, 100 mM KCl, 2.5 mM $MgCl_2$, 0.25% Triton X-100, 1 mM DTT) plus 2× cOmplete, EDTA-free protease inhibitor mix (Roche) and 1 mM PMSF and cleared by 15 min centrifugation at 19,000×g. Brn1-Protein A fusion proteins were purified by addition of 25 µl (bed volume) IgG sepharose FF (GE Healthcare) for 2 h at 4°C, followed by three 10 min wash steps in EBX (low salt) or one 10 min wash step in EBX and two 10 min wash steps in EBX + 200mM KCl (high salt), and eluted by 5 min incubation at 95°C in 100 µl 1× Laemmli loading buffer.

For the purification of endogenous condensin complexes, 2×10^3 OD_{600} cells were resuspended in 7 ml lysis buffer (50 mM TRIS-HCl pH 8.0, 100 mM NaCl, 2.5 mM $MgCl_2$, 0.15% Triton X-100, 1 mM DTT) plus 1× cOmplete, EDTA-free and 1 mM PMSF, snap-frozen as pellets in liquid nitrogen, and broken by cryogenic lysis in a freezer mill (Spex). Cell extracts were cleared by 15 min centrifugation at 45,000×g at 4°C. Ten µl Anti-V5 tag antibody (AbD Serotec) were added for 5 h at 4°C, followed by addition of 50 µl (bed volume) of Protein G dynabeads (Invitrogen) for 16 h at 4°C. Dynabeads were washed 5 times with lysis buffer and bound proteins eluted by 5 min incubation at 95°C in 25 µl 1× loading buffer.

Chromosome spreads, ChIP-qPCR, and ChIP-seq

Chromosome spreads and ChIP-qPCR were performed as described (Cuylen 2011), with the exception that fixation for ChIP-qPCR was performed in 3% (v/v) formaldehyde at room temperature. Primers for the *CEN4* locus were TGGTGTGGAAGTCCTAATATCG and TGCATGATCAAAAGGCTCAA. Primers for the rDNA locus were TTTCTGCCTTTTTCGGTGAC and TGGCATGGATTTCCCTTTAG.

For ChIP-seq analysis of PK_6-tagged Brn1, chromatin from asynchronous yeast cells was digested with 160 U micrococcal nuclease (Worthington Biochemicals) and purified using a MinElute PCR purification kit (Qiagen). Samples combined from three independent experiments were sequenced on a MiSeq Desktop Sequencer (Illumina). Paired-end sequencing reads were mapped to the *S. cerevisiae* genome (http://yeastgenome.org/ version R64-1-1) using bowtie 2, v2.1.0 with default settings (Langmead 2012). Reads with identical boundaries were discarded as PCR duplicates and the central position of each paired read mapping uniquely to the genome (mapq > 10) was used for computing the sequencing coverage. Except for Fig. 6d, duplicate reads were also removed from the region of chromosome XII containing the rDNA (coordinates 451,000–468,500), since the repetitive nature of this region would not have made it possible to distinguish independent fragments from duplicate reads. Library size was normalized to one million reads and coverage expressed as reads per million (rpm = number of mapped reads for each chromosomal coordinate point / total number of mapped reads × 10^6). H2A.Z ChIP-seq data (Htz1-TAP) was downloaded from GEO (GSE47073) and processed as described for Brn1-PK_6. Nucleosome position (Mavrich 2008) and H2A.Z-enriched nucleosome position (Albert 2007) datasets were downloaded from SGD (http://yeastgenome.org) to classify sub-

regions of the budding yeast genome as nucleosome-depleted or as nucleosome-enriched. To exclude regions with weakly bound or not well-positioned nucleosomes from the analysis, nucleosome depleted regions were defined as those DNA regions located between adjacent nucleosomes with sizes between 10 and 100 bp. Brn1-PK_6 binding was determined independently for each chromosome, and the statistical analysis to test whether Brn1 binds preferentially to the regions classified as nucleosome-enriched or -depleted was performed using R and Bioconductor (http://www.bioconductor.org). To infer differential signals between genome-wide binding sites of Brn1-PK_6 and Brn1(M1 M2 M4)-PK_6, the DESeq2 package for R/Bioconductor was used (Anders 2010).

Purification and chromosome binding of human condensin complexes

Single or multiple point mutations (see Supplementary Table 4) were introduced into pC1-Flag-EGFP-CAP-H or Flag-EGFP-CAP-H2 (Gerlich 2006) to perform transient transfections of Flp-In^{TM}-293 HEK cells (Life Technologies). Approx. 2×10^6 cells seeded in a 60 mm petri dish were treated with transfection mix (2 µg plasmid DNA, 6 µl lipofectamine 2,000 (Invitrogen), 100 µl Opti-MEM media (Life Technologies)) and incubated for 6 h. Opti-MEM media was then replaced with high-glucose DMEM media (Life Technologies) supplemented with 10% serum, 1% PenStrep (Invitrogen), 1% glutamine (Invitrogen). Cells were harvested after 18 h with a cell scraper and resuspended in 300 µl Cell Lytic M buffer (Sigma) supplemented with 2 mM DTT, 2× cOmplete EDTA-free protease inhibitor mix (Roche), 1 mM PMSF. Equivalent amounts of cleared protein extract were incubated for 2 h at 4°C with 5 µl anti-Flag antibody (monoclonal M2, Sigma) and then overnight with 50 µl protein G dynabeads (Invitrogen). Conjugated beads were washed twice with Cell Lytic M buffer supplemented with 2 mM DTT and 1 mM PMSF and bound proteins were eluted win 60 µl 2× loading buffer. Antibodies used for western blotting against CAP-H, CAP-G, CAP-D2, CAP-H2, CAP-D3, Smc2, and Smc4 were obtained from Bethyl Laboratories (A300-603A, A300-602A, A300-601A, A302-275A, A300-604A, A300-058A, A300-064A) and against CAP-G2 was obtained from Abgent (WA-AP17069c.80).

Imaging was performed with HeLa Kyoto H2B-mCherry cells (Neumann 2010). Cells were seeded into 35 mm dishes (MatTek), arrested with 100 ng/mL nocodazole, and transfected at 50-70% confluency as described above. Fresh medium containing 100ng/ml nocodazol was added 5-12 h before imaging. Cells were washed once and then imaged in 20 mM HEPES-KOH pH 7.4, 115 mM NaCl, 1.2 mM $CaCl_2$, 1.2 mM $MgCl_2$, 1.2 mM K_2HPO_4, 2 g/l D-glucose. Images were acquired at 37°C on a Zeiss LSM 780 microscope in 16-bit mode with 4 lines averaging with a Plan-Apochromat 63×/1.40 oil DIC M27 objective. Excitation and emission wavelengths were: 488 nm and 520–560 nm for EGFP or 561 nm and 580–650 nm for mCherry. All used cell lines were tested for mycoplasma contamination.

Image analysis

Dual color images of mitotic cells were analyzed with the CellProfiler software (Carpenter 2006). Background levels in the EGFP channel were measured outside cells and subtracted globally. Subsequently, a median filter was applied to correct for noise and fluorescence signals not belonging to the central mitotic cell were automatically removed based on their limited spatial extend using a morphological opening filter. The remaining signal was used to segment the cell by means of a manual threshold. Chromosomes were segmented using a manual threshold on the H2B channel after applying a median filter. Mean intensity signals were then measured in (i) the chromosome regions and (ii) the intracellular region excluding the chromosome regions (i.e. the cytoplasmic region) of background-subtracted but otherwise unfiltered EGFP images.

ATPase assays

ATPase assays were performed as described (Arumugam 2006) using 0.5 µM Smc2–Smc4 dimer, with or without 1.5 µM non-SMC subcomplex and/or 10 nM linearized 6.5 kb plasmid DNA, in 20 mM TRIS-HCl pH 7.8, 150 mM NaCl,

12.5 mM $MgCl_2$, 1.25 mM ATP (plus 33 nM α-^{32}P ATP; Hartmann Analytic), 1mM DTT. Ten microliter reactions were incubated at 30°C and 1 µl spotted onto PEI cellulose F TLC plates (Merck) every 5 min for 25 min. TLC plates were developed in 0.5 M LiCl, 1 M formic acid, exposed to phosphorimager plates and analyzed using a Typhoon FLA-7000 scanner. ATP hydrolysis rates were calculated from the ADP/ATP ratios of time points in the linear range of the reaction.